

Effect of Friction Stir Welding on Mechanical Properties and Formability of Aluminum Alloy-AA1100

Manish Singh¹, Pankaj Kumar Singh², Mandeep Kumar^{3*}, Parveen Kumar³, Surendra Singh⁴

¹ Department of Mechanical Engineering, Poornima University, Vidhani Vatika Road, 303905 Jaipur, Rajasthan, India

² Department of Mechanical Engineering, Indian Institute of Technology (BHU), 221005 Varanasi, India

³ Department of Mechanical Engineering, Chandigarh Engineering College, Chandigarh Group of Colleges, Jhanjeri, Mohali-140307, Punjab, India

⁴ Department of Mechanical Engineering, Bakhtiyarpur College of Engineering, 803212 Bakhtiyarpur, India

* Corresponding author, e-mail: mandeepkumar3636@gmail.com

Received: 11 November 2024, Accepted: 09 December 2024, Published online: 12 December 2024

Abstract

This study investigates the influence of friction stir welding (FSW) on the mechanical properties and formability of thin aluminum alloy sheets for automotive applications. The feasibility of a novel technique, pinless FSW, for joining aluminum sheets was demonstrated. Defect-free welds were successfully achieved using parameter sets R1 (450 rpm, 80 mm/min, 8 mm), R4 (560 rpm, 160 mm/min, 8 mm), and R7 (710 rpm, 250 mm/min, 8 mm). The welded region exhibited an outward material flow due to the stirring action of the FSW tool. Microhardness measurements were conducted in the transverse direction of the weld and along the depth from the top to the bottom at the weld center. Hardness values exhibited variation from the weld zone centerline to the heat-affected zone (HAZ). Lower hardness values were observed at the center of the weld zone, whereas higher hardness values were recorded in the HAZ. The transverse and longitudinal tensile properties of the welds were evaluated at room temperature. The tensile tests revealed that the welded samples failed outside the weld region. To assess the ductility of the FSW welded samples, formability tests were performed, indicating an increase in ductility within the welded area.

Keywords

friction stir welding, aluminum alloy, mechanical properties, limiting dome height, formability

1 Introduction

The welding of aluminum alloy is very difficult because of their high thermal conductivity and high reflection. Due to this many researchers' attention attracted towards improvement of aluminum alloy welding. The tungsten inert gas welding (TIG) is one of the prominent welding technologies which is used for the welding of aluminum alloy. TIG welding is an arc welding process that achieves the coalescence of metals through the application of heat generated by an electric arc established between a non-consumable tungsten electrode and the base metal [1]. In this process, the tungsten electrode, which does not melt during welding, is shielded by an inert gas. The electric arc consists a high temperature conducting plasma, which provides the necessary thermal energy needed to melt both the base and filler material. The high welding temperatures inherent in fusion welding process, such as TIG welding [2], result in the formation of a large

heat-affected zone (HAZ) and this HAZ can significantly alter the mechanical properties of the welded materials, including tailor welded blanks [3].

To avoid the issues associated with large HAZ in TIG welding, laser welding can be employed. Laser welding involves focusing a monochromatic light beam on the butt seam of two sheets producing a precise and concentrated heat source. This process offers several advantages for tailor welded blanks (TWBs), including the elimination of the need for filler material, the production of the narrow weld bead, and reduced heat input. However, developing TWBs for aluminum and magnesium alloys presents several challenges [4, 5]. These difficulties stem from the high reflectivity of these materials, low molten viscosity and inherent oxide layer. Conventional laser welding techniques often result in hot cracking within the fusion zone and the poor coupling of the laser energy during welding process.

As a novel welding technology for TWBs, friction stir welding (FSW) has been primarily developed for aluminum alloys. During the FSW process, heat is generated through two primary mechanisms; friction between the tool and the workpiece, and plastic deformation of the material. A portion of the plastic deformation energy is stored within the thermo mechanically affected zone (TMAZ) as increased defect densities [6].

FSW is a solid-state, hot-shear joining process in which a rotating tool with a shoulder and a pin traverses along the butting surfaces of two rigidly clamped plates positioned, on a backing plate, as shown in Fig. 1 (a) [7]. The shoulder engages with the top surface of the workpiece, generating heat through friction at the shoulder surface, which in turn softens the material being welded [8]. This process induces severe plastic deformation and flow of the plasticized metal as the tool advances along the welding direction. The material is transported from the leading edge of the tool to the trailing edge, where it is consolidated to form a joint. While Fig. 1 (b) illustrates a butt joint, FSW can be employed to fabricate other joint types, such as lap joints and fillet joints.

In the FSW process, the tool advances along the weld joint at a constant translational speed U , while simultaneously rotating about its axis with an angular velocity ω . At any point on the tool-workpiece interface, the tangential speed v_r of the tool relative to the work piece is expressed as; $v_r = \omega r - U \sin \theta$, where r represents the radial distance from the tool-axis, and θ is the angle between the radial vector r and the welding direction [9]. The term $U \sin \theta$ can be neglected when ωr is significantly larger. Heat generation at the tool-workpiece interface occurs due to frictional interactions and plastic deformation within the TMAZ. The frictional heat generation is the product of the frictional force and the sliding velocity. The deformation heat results from the shear stress and the velocity of the workpiece material adhering to the tool as

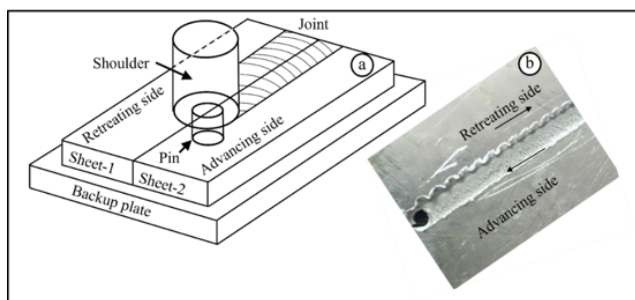


Fig. 1 Friction stir welding; (a) Schematic diagram and (b) FSW welded sample

it moves. The local heat generation rate due to friction, q' can be approximated as Eq. (1) [7]:

$$q' = \delta (\omega r - U \sin \theta) \mu_f P dA, \quad (1)$$

where δ is the extent of slip, μ_f is the friction coefficient and P is the local pressure applied by the tool on the elemental area dA . When $\delta = 1$, no material adheres to the tool, and all the heat generated at the interface is due to frictional forces. Conversely, when $\delta = 0$, the heat generation is entirely attributed to plastic deformation of the material.

In FSW process, the workpiece is divided into two sides; the retreating side (RS) and the advancing side (AS). The axis of the pin forms a work angle and a travel/tilting angle θ with respect to the normal direction of the blanks, as schematically shown in Fig. 2. The important process parameters for FSW are shown in Table 1 [10].

Welding parameters, such as tool rotation rate, traverse speed, spindle tilt angle, and target depth, are crucial for achieving sound and defect-free welds in the FSW process [11]. The FSW process induces a substantial temperature increase within and around the weld zone. A temperature increase of 400–500 °C has been recorded within the weld region of aluminum alloys [12]. This intense thermal exposure, coupled with plastic deformation leads to significant microstructural changes within the weld zone, including the formation of fine recrystallized grains ranging from 20 to 60 μm , the development of texture, and the

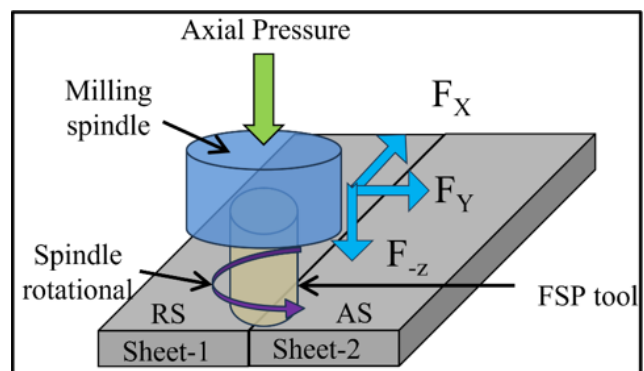


Fig. 2 Schematic illustration of the FSW process

Table 1 Important process parameters in FSW [10]

Parameter	Effects
Rotation speed	Friction heat, "Stirring", oxide layer breaking and mixing
Welding speed	Heat control
Shoulder diameter	Heat control
Depth of plunging	Heat control
Down force	Friction heat
Tilting angle	The appearance of the weld thinning

dissolution and coarsening of precipitates. Additionally, residual stresses are introduced with significantly lower magnitude compared to those found in traditional fusion welding methods. The observed softening effect in FSW is widely attributed to the dissolution and/or coarsening of the precipitates [13]. Furthermore, the hardness profile across the weld is asymmetric for all configurations. Generally, the AS of the weld typically exhibits higher hardness relative to the RS, which has been observed in other studies [14]. This discrepancy is attributed to the different deformations experienced by the material on both sides. Specifically, the material on the AS is subjected to more intense and prolonged interaction with the vortex velocity field [15]. This different interaction arises because the vortex directions on the RS oppose each other, whereas on the AS, they align in the same direction.

Therefore, the AS experiences more pronounced straining and grain refinement.

The weld can be divided into three different microstructural zones i.e., nugget region experiences intense plastic deformation and high-temperature exposure, resulting in fine and equiaxed recrystallized grains. Thermo-mechanically affected region is subjected to medium temperatures and deformation, characterized by deformed grains that have not fully recrystallized [16]. Heat-affected region experiences only thermal exposure, leading to precipitate coarsening without significant grain deformation. Compared to the traditional fusion welding techniques, FSW significantly enhances mechanical properties such as strength, ductility and fatigue resistance, and fracture toughness [17]. In friction stir welded aluminum alloys, up to 80% of the yield stress of the base material is retained, with failure typically occurring in the HAZ [18].

In assess the macroscopic performance of friction stir welded automotive TWB sheets, the hardening behavior, anisotropic yielding properties, and forming limit diagram (FLD) were characterized for both the base material and weld zones. The Bauschinger effect, transient hardening behaviors, and permanent softening during reverse loading were also analyzed. For the weld zones, hardening properties were determined using a combination of the rule of mixtures and direct measurements from sub-sized specimens [19].

Mechanical properties like hardness, yield strength, ultimate tensile strength, and total elongation are often initially utilized as a rough indicator of the formability of sheet metals. However, formability does not always correlate directly with ductility, particularly where cracking initiates at free surfaces. Furthermore, the size and shape

of the workpiece often prevent tension tests from being conducted in relevant directions. Consequently, alternative formability tests are employed.

Hecker developed a modified hemispherical cup test by scaling up the penetration size to 101.6 mm, adding a drawbead in the die plates near the die opening, and performing the tests under dry conditions [20]. This modified test is known as the limiting dome height (LDH) test. One of the most standard formability tests for evaluating sheet metal is the out-of-plane stretch forming test [21].

In this test, deformation is induced in an out-of-plane sheet sample by stretching it over a rigid hemispherical punch. Significant strain gradients are generated in out-of-plane stretch forming because of the combined effects of friction and curvature. The deformation is constrained by the tooling geometry, and bending strains are imposed on the sheet sample. The magnitude of these bending strains is dependent on the sheet thickness and the punch radius.

The welding technology for TWBs is well established; however, the forming characteristics of these TWBs are not yet fully understood [22]. The primary challenge lies in predicting how process parameters influence weld quality and how the location of welds affects the formability and mechanical properties of the TWBs. For this the detailed research experimentation, various mechanical tests and their analysis were presented in Sections 2 and 3 of this research articles.

2 Experimentation

In this experiment, a customized FSW setup was used, comprising a vertical milling machine, a fixture, and a control panel. Three different FSW tools with different configurations were used. The final dimensions of the tools have been tabulated in Table 2. High carbon alloy steel of EN31 grade was used as the FSW tool material. Aluminum alloy (AA1100), with a sheet thickness of 1.7 mm was used for the experimentation. The elemental composition of AA1100 is presented in Table 3. For this,

Table 2 FSW tool dimensions

Tool	Tool 1	Tool 2	Tool 3
Tool pin diameter (mm)	8	12	16
Tool pin length (mm)	10	10	10
Shank diameter (mm)	20	20	20
Shank length (mm)	55	55	55

Table 3 The chemical composition of aluminum alloy (AA1100) sheet

Elements	Al	Cu	Fe	Mn
Content	99.0–99.95%	0.05–0.20%	0.95% max	0.05% max.

the sheets were cut into strips of 170 mm × 52 mm × 1.7 mm using a shearing machine. After cutting, the edges of the strips were machined in shaper machine so that proper edges of the strips aligned during welding. FSW was carried out under a variety of process parameters; the trial run and machine availability were used to determine the values for each factor. For the process parameter optimization, Taguchi's (L9) array method was used. The optimized FSW process parameters are presented in Table 4.

All weld samples are shown in Table 5. Equation 1 shows that at higher tool pin diameters, increased tool rotation speed, and reduced welding speeds result in high heat generation, as evidenced by samples R2, R3, R5, and R8 shown in Table 5. High heat generation leads to excessive material flash during welding and increased sticking between the

strips and the backing plate, which is undesirable. The conditions of samples R6 (560 – 80 – 16) and R9 (710 – 160 – 16) were not feasible due to the combination of large tool diameter and lower welding speed. Samples R1 (450 – 80 – 8), R4 (560 – 160 – 8), and R7 (710 – 250 – 8) resulted in high quality welds, as shown in Table 5.



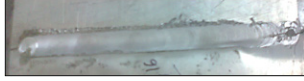


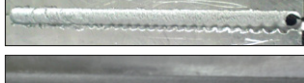
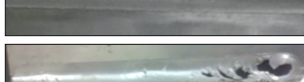


3 Mechanical properties

The mechanical and metallographic characteristics of the different specimens were examined following the fabrication of the samples, as depicted in Fig. 3. Metallographic samples were cut in the transverse direction of weld and mounted using epoxy resin. The samples were polished with different grade of emery papers ranging from 100 to 4000 grits, followed by soft polishing on cloth with alumina

Table 4 FSW process parameters optimized by Taguchi's array method

Welding run No.	Rotational speed (rpm)	Welding speed (mm/min)	Tool diameter (mm)	Depth of plunging (mm)
1	450	80	8	0.35
2	450	160	12	0.35
3	450	250	16	0.35
4	560	160	8	0.35
5	560	250	12	0.35
6	560	80	16	0.35
7	710	250	8	0.35
8	710	80	12	0.35
9	710	160	16	0.35

Table 5 List of prepared samples at different process parameters

Welding run	FSW parameters (tool rotational speed-welding speed-tool diameter)	Prepared sample	Result
R1	450 – 80 – 8		Good
R2	450 – 160 – 12		Poor/over heating
R3	450 – 225 – 16		Not possible due to over heating
R4	450 – 160 – 8		Good
R5	560 – 250 – 12		Poor/over heating
R6	560 – 80 – 16		Not possible due to over heating
R7	560 – 80 – 16		Good
R8	710 – 80 – 12		Poor/over heating
R9	710 – 160 – 16		Not possible due to over heating

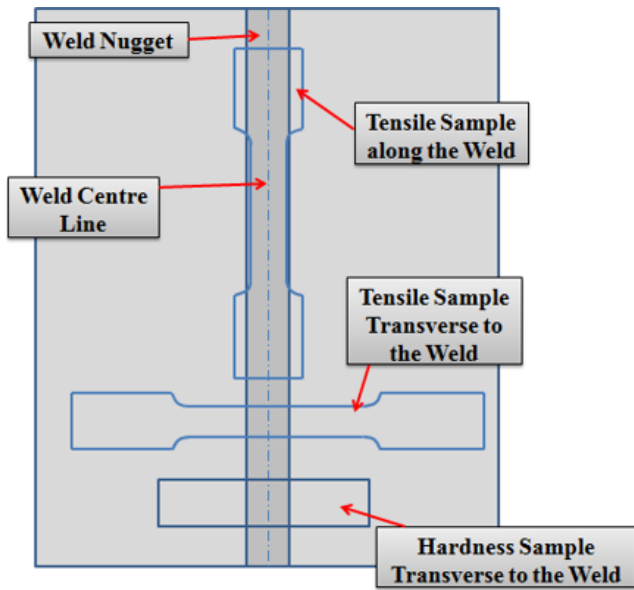


Fig. 3 Schematic of sample extraction for mechanical and metallurgical characterization

powder (Al_2O_3) of grades I, II and III, having particle sizes of 5, 3, and 1 μm , respectively. Subsequently, the samples were etched with Keller's reagent, comprising 2.5 % HNO_3 , 1.5 % HCl and 1 % HF , and 95 % water (by volume).

Vickers hardness test was performed on each sample in the transverse direction of the weld, covering the AS, weld nugget, and RS. Hardness, typically defined as a material's resistance to permanent indentation, was measured using a 100 g indentation load with a 10 sec dwell time. Microhardness test samples were prepared for each weld run, taken from the weld specimen across the weld region, covering the entire weld region, including the weld nugget zone and HAZ, as shown in Fig. 4.

The tensile tests were conducted as per ASTM E8/E8M-11 standard [23]. The tensile samples were cut along the weld line using wire EDM. Uniaxial tensile tests were performed on each sample to determine the ultimate tensile strength and elongation. These important parameters, obtained from standard tensile testing, are useful for selecting suitable engineering materials and welds for various applications. Tensile tests were carried out in both transverse and longitudinal directions to identify the

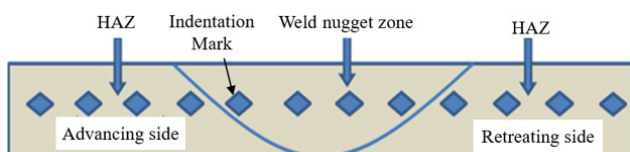


Fig. 4 Schematic of cross-sectional view of a microhardness test specimens

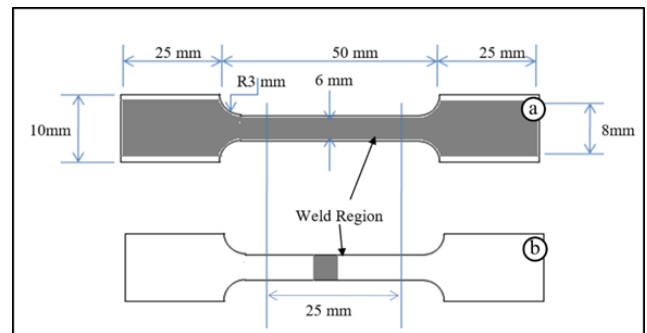


Fig. 5 Sub-size specimens used in tensile tests of TWBs; (a) longitudinal specimen and (b) transverse specimen [24]

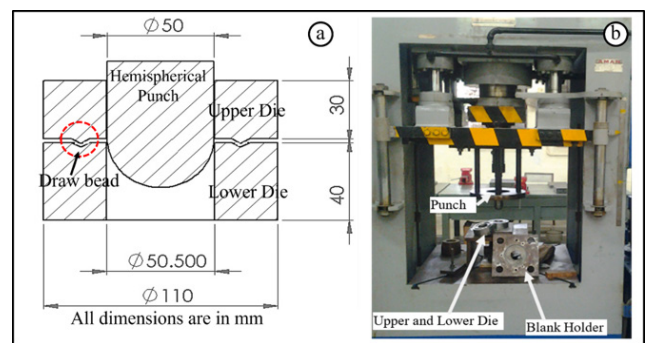


Fig. 6 Experimental setup of stretch forming tests; (a) schematic diagram of stretch forming tool and (b) stretch forming machine

weakest region of the weld and evaluate the strength of the weld zone. Two tensile test specimens were prepared from each weld run sample, as shown in Fig. 5 [24]. To evaluate the formability performance of friction, stir welded sheets, the LDH test was performed using a hemispherical punch with 50 mm diameter (Fig. 6 (a)) on a double action 100-ton hydraulic press, as shown in Fig. 6 (b).

For LDH tests, square specimens of size 100 mm \times 100 mm, as shown in Fig. 6 (a), were cut from the FSW samples. A circular draw-bead was provided on the dies with an 80 mm diameter (red circled in Fig. 6 (a)) to restrict the metal flow from the flange region into the die, thereby ensuring complete clamping of the blank at the draw-bead. Since the specimen thickness is greater than the draw-bead diameter, so this is the case of biaxial stretching. All tests were conducted under dry conditions with a punch speed of 20 mm/min. An optimum blank holding force ranging from 5 to 6 tons was applied to the upper die. Experiments were stopped upon the visible onset of necking, as shown in Fig. 7 (b). The dome height of each specimen was measured using a height gauge with a least count of 0.02 mm.

A FLD is a plot of the major stress versus the minor strain within the plane of the sheet for different strain ratios. At each minor strain, there is a corresponding limiting major

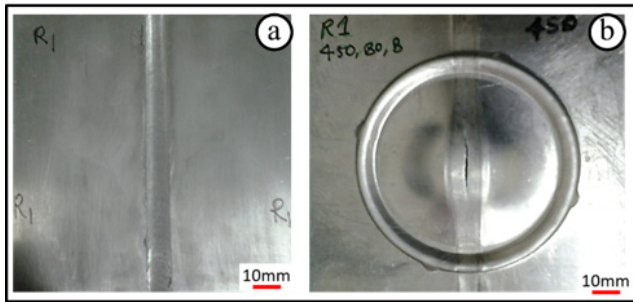


Fig. 7 LDH tests specimen; (a) before testing and (b) after testing (separation of the weld line observed during stretch forming)

strain that can be achieved before failure [11]. The locus of points representing the limiting major strain/minor strain ratios constitutes FLD, representing a boundary below which "safe" ratios of major-to-minor strain are maintained. For FLD tests, square specimens of size 100 mm × 100 mm were cut from the FSW samples. To measure surface strains, grid circles with a diameter of 5 mm were laser-engraved by laser on the specimens, as shown in Fig. 8.

The LDH of the entire deformed specimen in stretch forming was measured by a vernier height gauge with a least count of 0.02 mm. The major and minor diameters of deformed ellipse were measured by a travelling microscope with a least count of 0.001 mm. The variations in major and minor strains both along and across the weld were measured for all combinations to plot strain distribution profiles. The weld line movement was measured by determining the coordinates of approximately eleven points along the weld line of the deformed specimen.

4 Results and discussion

4.1 Microhardness

The microhardness analysis revealed that the average width of the weld zone (weld nugget zone and HAZ) extends approximately 3 to 4 mm beyond the weld nugget zone on both sides, resulting in a total width of approximately 14 mm for an 8 mm diameter tool. The hardness profiles for all welds configurations are shown in Fig. 9, demonstrating a pronounced heterogeneous nature in hardness distribution induced by welding. This heterogeneity is attributed to the well-discussed softening effect of FSW, which is primarily due to dissolution and/or coarsening of precipitates.

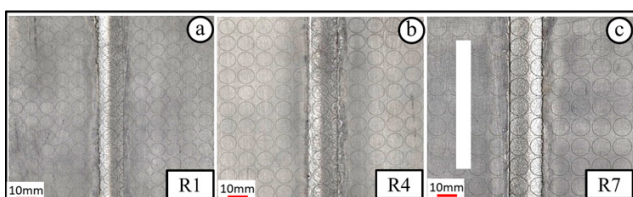


Fig. 8 FLD tests specimens; (a) R1, (b) R4, and (c) R7

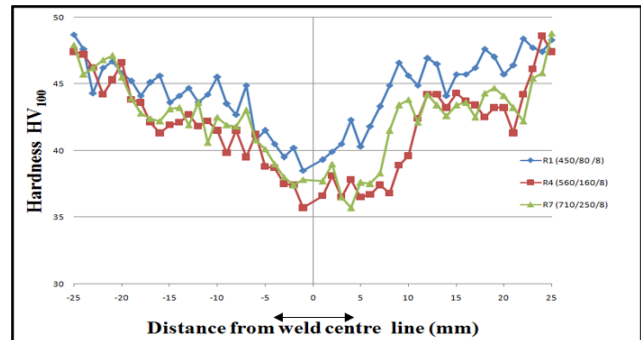


Fig. 9 Microhardness profile across the weld in TWBs samples

Furthermore, the hardness profile is asymmetrical across all configurations, with the AS generally exhibiting higher hardness compared to the RS. This has been observed in other findings as well and is a consequence of the differing deformations experienced on each side. The material on the AS is subjected to more extensive and longer influence by the vortex velocity field, as the directions of the vortex velocity align on the AS but diverge on the RS. Therefore, the straining and grain refinement are more pronounced on the AS.

4.2 Tensile test

Sub sized tensile specimens from the FSW welded samples were tested in both longitudinal and transverse directions. Transverse tests were performed to evaluate the strength of the weld region and to ensure that the selected weld parameters for the FSW welding were optimal. Failure was observed in the weld nugget zone because thickness of the joint reduced in this region due to plastic flow of metal across the weld movement direction which is known as flash. The fractured specimens from the base metal, as well as those from transverse and longitudinal tensile tests of the weld region, are shown in Fig. 10.

The standard tensile properties including, 0.2% offset yield strength, ultimate tensile strength, and elongation for the base metal, transverse to the weld, and longitudinal to the weld for each run, as determined from the tensile tests, are given in Table 6.

From Table 6, it is observed that the yield strength and ultimate tensile strength of the weld (i.e., the longitudinal direction/along the weld (LW) and the transverse direction/across the weld (TW) are lower than those of the base metal. However, the percentage elongation of the weld metal exceeds that of the base metal in both the longitudinal and transverse directions. Additionally, it is observed that the percentage elongation of the longitudinal weld is greater than that of the transverse weld but the yield strength and

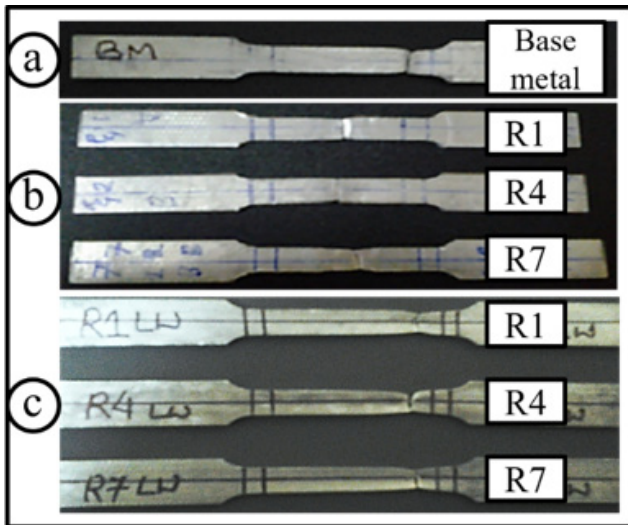


Fig. 10 Fracture specimen after tensile tests; (a) base material, (b) across transverse to the weld, and (c) along longitudinal to the weld

Table 6 Mechanical properties of base metal and weld metal

Welding run	YS (MPa)	UTS (MPa)	Elongation (%)
Base metal	110.51 ± 15.4	118.07 ± 17.3	8.03 ± 1.2
R1 TW	82.87 ± 11.8	92.77 ± 13.1	12.06 ± 1.4
R4 TW	83.50 ± 12.2	93.43 ± 14.2	9.56 ± 1.8
R7 TW	82.87 ± 10.4	89.64 ± 12.5	10.53 ± 2.1
R1 LW	83.04 ± 11.7	91.50 ± 13.6	23.69 ± 3.4
R4 LW	84.75 ± 12.3	93.62 ± 15.1	33.21 ± 5.3
R7 LW	80.28 ± 11.4	91.81 ± 14.2	27.4 ± 4.5

ultimate tensile strength of the welds in both the longitudinal and transverse directions are approximately equal.

The results can be verified by examining the stress – strain curves shown in Fig. 11 and Fig. 12. It is evident from these curves that the sample R1 (450 rpm, 80 mm/min, 8 mm) yields superior tensile strength with lower elongation. Conversely, an increase in tool rotation speed results in higher percentage elongation. Notably, the sample R7 (710 rpm, 250 mm/min, 8 mm) shows a balanced performance, offering both high tensile strength and good ductility compared to the other samples tested.

4.3 Formability

The formability of FSW welded and base metal specimens was examined by measuring the dome height through LDH tests.

4.3.1 LDH in biaxial stretching

The biaxially stretched samples subjected to the FSW are depicted in Fig. 13. Each parameter set was tested with three samples, and the average LDH for each set is shown in Table 7. The results indicate a distinct trend: the LDH

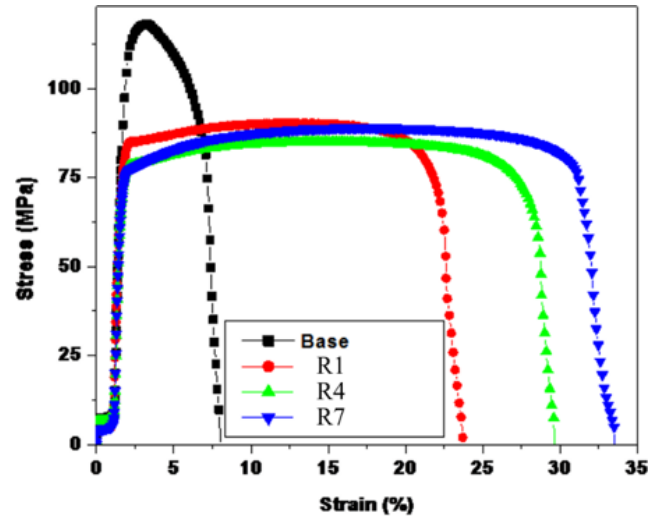


Fig. 11 Stress v/s strain curve of the longitudinal direction of the weld for each run along with base metal

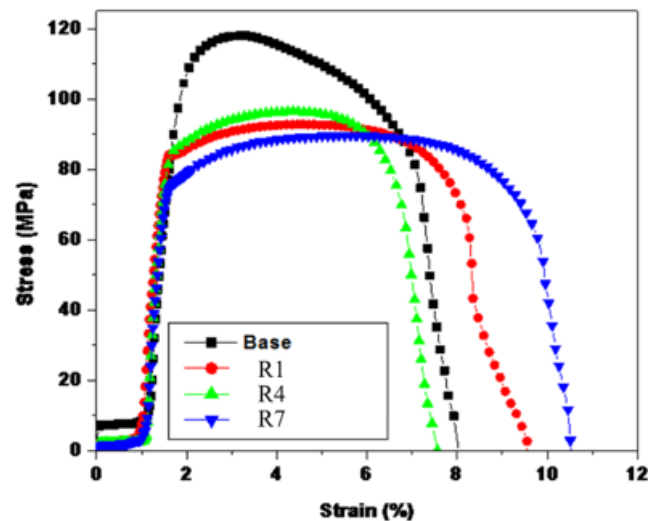


Fig. 12 Stress v/s strain curve of transverse direction of the weld for each run along with base metal

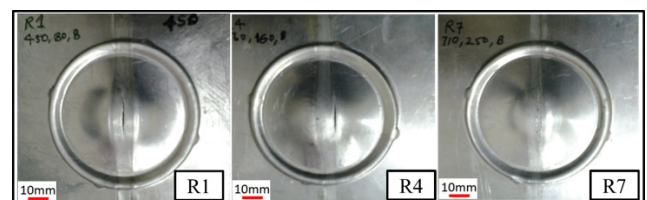


Fig. 13 LDH test specimens after stretching under various parameter sets

Table 7 LDH under various parameter sets

Sample	R1	R4	R7
Average LDH (mm)	11.04 ± 1.2	12.02 ± 1.5	12.04 ± 1.6

measurements show that as the rotational speed of the FSW increases, there is a corresponding rise in ductility. This increase in LDH with higher tool rotational speed is attributed to enhanced heat generation during the welding process. The elevated heat levels result from intensified

frictional forces and increased plastic deformation due to the higher rotational speed of the tool.

4.3.2 Strain distribution in biaxial stretching

Understanding the capability of a material to distribute strains is crucial for comprehending its formability. This includes not only determining the maximum punch height but also understanding spring back and shape fixation. Fig. 14 depicts the FSW welded samples subjected to different parameter sets (with grid markings) after biaxial stretching. The LDH values for the tested samples are summarized in Table 8. A typical strain distribution profile for a stretch-formed sample under different parameter sets is depicted in Fig. 15. Strain distributions of stretch-formed

base metal samples reveal two peaks symmetrically positioned on either side of the pole (Fig. 15 (a)). In the pole region, minimal deformation occurs due to friction between the punch and the sheet. Notably, at these peaks, major strains significantly surpass minor strains owing to geometrical constraints.

The strain distribution profiles of major and minor strain variations on the stretch-formed samples of the FSW welded samples at different parameter sets are illustrated in Fig. 15 ((a)-(d)). Analysis of the curves from the weld specimens (R1, R4, and R7) indicates that strain levels at the pole are higher compared to the base metal region (weld region). This phenomenon is attributed to factors such as increased ductility, reduced weld strength, and diminished thickness at the pole.

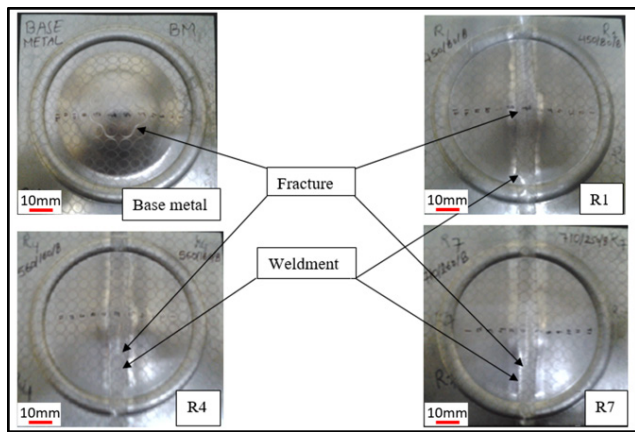


Fig. 14 Deformed FSW welded samples under various parameter sets (with grid marking) for biaxial stretching

Table 8 LDH of FSW welded specimens for different parameter sets and base metal specimens in biaxial stretch forming

Specimen	Base metal	R1	R4	R7
Average LDH (mm)	18.04 ± 1.8	11.32 ± 1.5	11.56 ± 1.3	11.98 ± 1.6

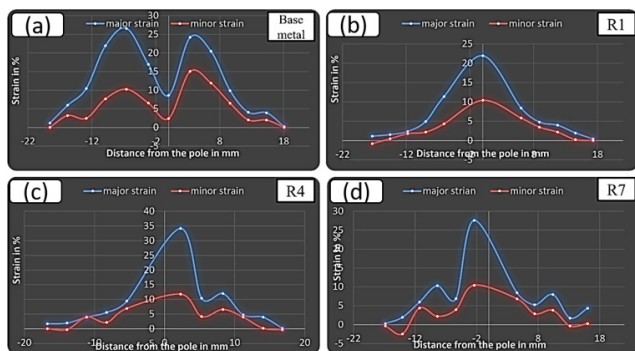


Fig. 15 Major strain and minor strain distribution of (a) base metal, (b) R1, (c) R4, and (d) R7 stretch-formed samples

5 Conclusions

The following conclusions are drawn from the results:

- The FSW process was used to join the AA1100 sheets. It is concluded from the results that the optimum range of tool rotation is between 450 and 710 rpm. Rotational speed below 450 rpm result in insufficient heat generation, leading to produce not good joint quality. Conversely, rotational speeds more than 710 rpm cause flushing.
- At a constant rotational speed, an increase in travel speed leads to wormhole initiation near the bottom of the weld. The size of these wormholes increases with travel speed due to inadequate material flow towards the bottom of the weld.
- Tensile tests were performed to determine the mechanical properties of the AA1100 sheets as well as the weld region (i.e., longitudinal and transverse directions) of the FSW welded samples. It was observed that the percentage elongation of the weld in the longitudinal direction is significantly higher than compared to the base metal.
- Hardness in the AS of the HAZ is greater than in the RS because grain refinement is more pronounced on the AS.
- From the LDH tests, it was observed that the LDH in sample R7 (710 rpm, 250 mm/min, 8 mm) is higher than in samples R1 (450 rpm, 160 mm/min, 8 mm) and R4 (560 rpm, 160 mm/min, 8 mm). In the LDH tests, failures occurred in the weld region in some samples and in the HAZ in others.

References

- [1] Sarolkar, A. D., Kolhe, K. P. "A Review of (GTAW) Gas Tungsten Arc Welding and its Parameters for Joining Aluminium Alloy", *IJSART*, 3(8), pp. 361–368, 2017.
- [2] Singh, M., Singh, R. K. R., Gupta, G. "Investigation of Frictional Deformation on Mechanical and Metallurgical Properties of Ni-based Functionally Graded Materials Developed by Wire and Arc Additive Manufacturing", *Journal of Materials Engineering and Performance*, 2024.
<https://doi.org/10.1007/s11665-024-09136-9>
- [3] Habibi, M., Hashemi, R., Tafti, M. F., Assempour, A. "Experimental investigation of mechanical properties, formability and forming limit diagrams for tailor-welded blanks produced by friction stir welding", *Journal of Manufacturing Processes*, 31, pp. 310–323, 2018.
<https://doi.org/10.1016/j.jmapro.2017.11.009>
- [4] Kim, D., Lee, W., Kim, J., Kim, C., Chung, K. "Formability evaluation of friction stir welded 6111-T4 sheet with respect to joining material direction", *International Journal of Mechanical Sciences*, 52(4), pp. 612–625, 2010.
<https://doi.org/10.1016/j.ijmecsci.2010.01.001>
- [5] Singh, P. K., Kumar, S., Jain, P. K. "Effect of cryogenic grinding on surface characteristics of additively manufactured Ti-6Al-4V alloy", *Surface Topography: Metrology and Properties*, 11(1), 015014, 2023.
<https://doi.org/10.1088/2051-672X/acad16>
- [6] Liu, F. C., Hovanski, Y., Miles, M. P., Sorensen, C. D., Nelson, T. W. "A review of friction stir welding of steels: Tool, material flow, microstructure, and properties", *Journal of Materials Science & Technology*, 34(1), pp. 39–57, 2018.
- [7] Nandan, R., DebRoy, T., Bhadeshia, H. K. D. H. "Recent advances in friction-stir welding – Process, weldment structure and properties", *Progress in Materials Science*, 53(6), pp. 980–1023, 2008.
<https://doi.org/10.1016/j.pmatsci.2008.05.001>
- [8] Sahu, P. K., Pal, S., Pal, S. K., Jain, R. "Influence of plate position, tool offset and tool rotational speed on mechanical properties and microstructures of dissimilar Al/Cu friction stir welding joints", *Journal of Materials Processing Technology*, 235, pp. 55–67, 2016.
<https://doi.org/10.1016/j.jmatprotec.2016.04.014>
- [9] Heidarzadeh, A., Mironov, S., Kaibyshev, R., Çam, G., Simar, A., Gerlich, A., Khodabakhshi, F., Mostafaei, A., Field, D. P., Robson, J. D., Deschamps, A., Withers, P. J. "Friction stir welding/processing of metals and alloys: A comprehensive review on microstructural evolution", *Progress in Materials Science*, 117, 100752, 2021.
<https://doi.org/10.1016/j.pmatsci.2020.100752>
- [10] De, P. S., Kumar, N., Su, J. Q., Mishra, R. S. "Fundamentals of Friction Stir Welding", In: Lienert, T., Siewert, T., Babu, S., Acoff, V. (eds.) *Welding Fundamentals and Processes*, ASM International, 2011, pp. 186–200. ISBN 978-1-62708-174-0
<https://doi.org/10.31399/asm.hb.v06a.a0005637>
- [11] Singh, M., Singh, R. K. R., Gupta, D. "Effect of in-situ cooling during pressure and frictional deformation on mechanical and metallurgical properties of Ni-based functionally graded material developed by wire arc additive manufacturing", *Proceedings of the Institution of Mechanical Engineers, Part L: Journal of Materials: Design and Applications*, 238(1), pp. 50–64, 2024.
<https://doi.org/10.1177/14644207231183096>
- [12] Yaduwanshi, D. K., Bag, S., Pal, S. "Heat transfer analyses in friction stir welding of aluminium alloy", *Proceedings of the Institution of Mechanical Engineers, Part B: Journal of Engineering Manufacture*, 229(10), pp. 1722–1733, 2015.
<https://doi.org/10.1177/0954405414539297>
- [13] Zadpoor, A. A., Sinke, J., Benedictus, R., Pieters, R. "Mechanical properties and microstructure of friction stir welded tailor-made blanks", *Materials Science and Engineering: A*, 494(1–2), pp. 281–290, 2008.
<https://doi.org/10.1016/j.msea.2008.04.042>
- [14] Ma, Z. Y., Feng, A. H., Chen, D. L., Shen, J. "Recent Advances in Friction Stir Welding/Processing of Aluminum Alloys: Microstructural Evolution and Mechanical Properties", *Critical Reviews in Solid State and Materials Sciences*, 43(4), pp. 269–333, 2018.
<https://doi.org/10.1080/10408436.2017.1358145>
- [15] Kumar, M., Singh, R. K. R., Jain, V. "Effect of tool pin profiles on the properties of foamable precursor developed by friction stir processing", *Proceedings of the Institution of Mechanical Engineers, Part E: Journal of Process Mechanical Engineering*, 237(4), pp. 1367–1377, 2023.
<https://doi.org/10.1177/09544089221113562>
- [16] Kumar, M., Singh, R. K. R., Jain, V. "Characterization of mechanical and metallurgical properties of AA6063 foam developed by friction stir precursor deposition technique", *Journal of Adhesion Science and Technology*, 37(18), pp. 2608–2625, 2023.
<https://doi.org/10.1080/01694243.2022.2152405>
- [17] Singh, R. K. R., Rathod, D. W., Pandey, S. "Friction stir welding of nuclear grade SA508Gr.3Cl.1 and SS304LN dissimilar steels", *Proceedings of the Institution of Mechanical Engineers, Part C: Journal of Mechanical Engineering Science*, 232(21), pp. 3814–3822, 2018.
<https://doi.org/10.1177/0954406218799782>
- [18] Srivastwa, A. K., Singh, P. K., Kumar, S. "Experimental investigation of flow forming forces in Al7075 and Al2014 – A comparative study", *Materials Today: Proceedings*, 47, pp. 2715–2719, 2021.
<https://doi.org/10.1016/j.matpr.2021.02.781>
- [19] Chung, K., Lee, W., Kim, D., Kim, J., Chung, K.-H., Kim, C., Okamoto, K., Wagoner, R. H. "Macro-performance evaluation of friction stir welded automotive tailor-welded blank sheets: Part I – Material properties", *International Journal of Solids and Structures*, 47(7–8), pp. 1048–1062, 2010.
<https://doi.org/10.1016/j.ijsolstr.2009.12.022>
- [20] Miles, M. "Formability Testing of Sheet Metals", In: Semiatin, S. L. (ed.) *Metalworking: Sheet Forming*, ASM International, 2006, pp. 673–696. ISBN 978-1-62708-186-3
<https://doi.org/10.31399/asm.hb.v14b.a0005149>
- [21] Imam, M., Biswas, K., Racherla, V. "Effect of weld morphology on mechanical response and failure of friction stir welds in a naturally aged aluminium alloy", *Materials & Design*, 44, pp. 23–34, 2013.
<https://doi.org/10.1016/j.matdes.2012.07.046>
- [22] Krishnamraju, M., Reddy, P. V., Appalanaidu, B., Markendeya, R. "Mechanical behavior and forming characteristics of tailor-welded blanks of structural materials: a review", *Multiscale and Multidisciplinary Modeling, Experiments and Design*, 7(4), pp. 3133–3151, 2024.
<https://doi.org/10.1007/s41939-024-00422-6>

- [23] ASTM "ASTM E8/E8M-11 Standard Test Methods for Tension Testing of Metallic Materials", ASTM International, West Conshohocken, PA, USA, 2013.
https://doi.org/10.1520/E0008_E0008M-11
- [24] Chowrasia, M. K., Kumar, A., Banerjee, M. K., Pandel, U. "Effect of Aging on Structure and Properties of a Transformation-Induced Plasticity-Aided High-Manganese Steel", *Journal of Materials Engineering and Performance*, 29(1), pp. 648–661, 2020.
<https://doi.org/10.1007/s11665-020-04575-6>